AN OVERVIEW OF HEAT TRANSFER ENHANCEMENT BASED UPON NANOPARTICLES INFLUENCED BY INDUCED MAGNETIC FIELD WITH SLIP CONDITION VIA FINITE ELEMENT STRATEGY

Muhammad B. HAFEEZ*, Marek KRAWCZUK*, Hasan SHAHZAD**

*Faculty of Mechanical Engineering and Ship Technology, Institute of Mechanics and Machine Design, Gdansk University of Technology, ul. Narutowicza 11/12, 80-233 Gdańsk, Poland
**Faculty of Materials and Manufacturing, College of Mechanical Engineering and Applied Electronics Technology, Beijing University of Technology, 100 Pingleyuan, Chaoyang District, Beijing 100124, China

muhammad.bilal.hafeez@pg.edu.pl, marek.krawczuk.@pg.edu.pl, hasanshahzad99@hotmail.com

received 2 February 2022, revised 6 April 2022, accepted 10 April 2022

Abstract: The mathematical model of heat generation and dissipation during thermal energy transmission employing nanoparticles in a Newtonian medium is investigated. Dimensionless boundary layer equations with correlations for titanium dioxide, copper oxide, and aluminium oxide are solved by the finite element method. Parameters are varied to analyze their impact on the flow fields. Various numerical experiments are performed consecutively to explore the phenomenon of thermal performance of the combination fluid. A remarkable enhancement in thermal performance is noticed when solid structures are dispersed in the working fluid. The Biot number determines the convective nature of the boundary. When the Biot number is increased, the fluid temperature decreases significantly. Among copper oxide, aluminium oxide, and titanium oxide nanoparticles, copper oxide nanoparticles are found to be the most effective thermal enhancers.

Key words: magnetohydrodynamic flow, porous medium, nanofluids, heat transfer, thermal performance, convective boundary conditions, FEM

1. INTRODUCTION

Fluid flows in porous media have a variety of uses in everyday life, including oil movement in the soil, and fluid seepage through sands and rocks, among others. Numerous research on the impact of fluid flow and heat transport has been done in light of this fact. For example, [1] examined the function of porous media and nanoparticles in heat and mass transmission during homogeneous and heterogeneous chemical reactions. The effect of a magnetic field on the transport of heat energy in a Maxwellian fluid along the channel field, under the influence of the porous medium, was discussed in [2]. For example, in [3], the pore diameters of heterogeneous porous media were optimized during random convection inside a two-sided lid-driven cavity. Numerical solutions for improving heat conduction of water–iron oxide nanofluids in the presence of a porous medium were discovered in [4]. The effect of porous media on MHD natural convection in a cone containing cadmium telluride nanofluid was investigated in [5]. [6] investigated the effects of nano-sized particles on heat energy transport during convective heat transfer in magnetohydrodynamic (MHD) flow in the presence of sinusoidal resistive force generated by porous media. Refer [7] reported the numerical solution of MHD nanofluid flow in porous media, including the effects of velocity slip and non-linear thermal radiation using the finite element technique (FEM).

An electrically conducting fluid subjected to a magnetic field behaves substantially differently from an electrically conducting nanofluid due to the Lorentz force's influence on fluid movement and heat energy transmission. MHD flow occurs when a fluid is exposed to a magnetic field, as has been extensively addressed. [8] examined the heat transport in a fluid filled chamber under the influence of an external magnetic field, for example. The transmission of energy during MHD fluid flow around a cylinder was investigated in [9. The effects of magnetic fields on the transmission of momentum and heat energy in a radiative fluid containing nanoparticles were discussed in [10]. In [11], we performed a computational simulation to look at the increase in heat transmission in MHD flow over a moving surface. [12] investigated the effects of magnetic field and nanoparticles on current and ion slip in three-dimensional flow. [13] used numerical simulation to model two-phase MHD non-Newtonian flow between nanoparticle-filled plates. In [14], the numerical solution for an unstable MHD maxwell nanofluid flow over a stretching sheet in the presence of thermo-diffusion and radiation was obtained using the FEM. The MHD free convection of a nanofluid flowing across a vertical cone was studied using finite element analysis in [15].

Many academics working in the field of thermal system design are constantly coming up with new ways to create more efficient thermal systems. The most frequent method involves the dispersion of metallic nanoparticles in a base liquid, and several aspects of this process have already been discussed. Diffusion of nano-sized particles in the base liquid has improved thermal performance and generated a more efficient working fluid than the base fluid, both experimentally and conceptually. Nanofluids are these forms of fluids. The invention of nanofluids has inspired research-

ers, and various papers have been published. For example, in [16], the authors discussed an increase in the transport of heat energy in an electrically conducting fluid exposed to a magnetic field. They used the lattice Boltzmann method to analyze the underlying physics. The impact of nano-sized alumina particle dispersion on heat energy and momentum transfer in MHD fluid was investigated in [17], which discussed an increase in the wall heat flux due to a rise in thermal conductivity. In [18], we looked at Walter B rheology and applied mathematical models to improve mixed convective heat and mass transmission. They used numerical simulations to look into different physical aspects. The influence of metallic nano-sized particles on the efficacy of thermal conduction of the working fluid was studied theoretically in [19]. [20] investigated the transport mechanism in the three-dimensional flow of an MHD fluid incorporating nano-sized particles and found a considerable improvement in the working fluid's thermal performance. The influence of nano-sized solid objects on the thermal effectiveness of a working fluid was explored using natural convection in a hollow [21] with an elliptical heater. The best analytic approach utilized in [22] is to determine a nanomaterial's thermal performance. They also discovered the effect of heat dissipation on temperature distribution in nanomaterials and an increase in working fluid efficiency due to the inclusion of metallic nanostructures. The effects of porous media and thermal radiation on the transmission of energy and momentum in a liquid containing solid nanoparticles were investigated in [23]. A mathematical model for homogeneous–heterogeneous chemical reactions during mass transport of MHD Eyring–Powell fluid on a spinning disc was developed by an author [24]. [25] looked studied the effects of porous media and non-linear thermal radiation on the thermal properties of a fluid subjected to nanostructure dispersion in mass transport, taking chemical processes into account. [26] employed mathematical models to investigate the effect of nanoparticle hybridity on the effectiveness of thermal conductivity of fluid across a moving surface when heat dissipation is significant. [27] investigated the effect of metallic nanoparticle hybridity on the thermal performance of a working fluid subjected to an external magnetic field using mathematical modeling. [28] investigated the flow across a revolving disc with an external magnetic field and thermal radiations. Readers are encouraged to look up prior works [29-32] and their references for further information on nanofluids and their applications. The effects of an induced magnetic field and changes in thermal conductivity on the flow of a second-grade fluid in the presence of a porous medium have also been studied [34-35].

This research aims to investigate the thermal properties of a nanofluid under convective boundary circumstances (BCs). This project is divided into five pieces. In Section 2, mathematical modeling is explained. Section 3 discusses the solution technique. Section 4 presents and discusses the outcomes. Finally, the paper is concluded with a short conclusion.

2. PHYSICAL SETUP AND DESCRIPTION

Let us consider the dispersion of three types of nanometallic structures, i.e., CuO, Al_2O_3 and TiO_2, in water, in order to investigate the increase in its thermal conductivity. Nano-water is subjected to an applied magnetic field. The nano-water mixture over a hot vertical surface experiences convection. This nano-water mixture is also assumed to be a heat-generating mixture. The buoyant force is significant under the Boussinesq calculation. The fluid flows through a porous medium and hence experiences a resistive force. The simplified partial differential equations PDE are as follows [33]:

$$\frac{\partial u}{\partial x}+\frac{\partial v}{\partial y}=0, \tag{1}$$

$$u\frac{\partial u}{\partial x}+v\frac{\partial u}{\partial y}=\frac{\mu_{nf}}{\rho_{nf}}\frac{\partial^2 u}{\partial y^2}+\beta_{nf}g\left(T_f-T_\infty\right)-\frac{\sigma_{nf}{B_0}^2u}{\rho_{nf}}-\mu_{nf}\frac{u}{k_1}, \tag{2}$$

$$u\frac{\partial T_f}{\partial x}+v\frac{\partial T_f}{\partial y}=\frac{k_{nf}}{(\rho c_p)_{nf}}\frac{\partial^2 T_f}{\partial y^2}+\frac{\mu_{nf}}{(\rho c_p)_{nf}}\left(\frac{\partial u}{\partial y}\right)^2+\frac{\sigma_{nf}{B_0}^2u^2}{(\rho c_p)_{nf}}+\frac{Q_0}{(\rho c_p)_{nf}}\left(T_f-T_\infty\right) \tag{3}$$

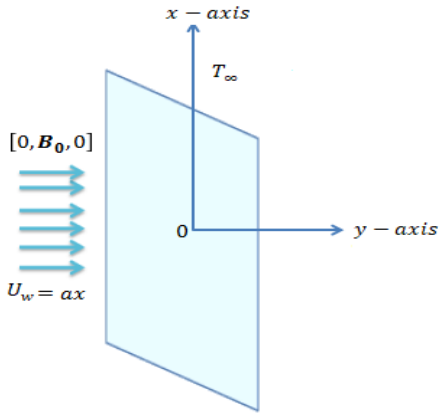

Fig. 1. Schematics - The physical arrangement and system of coordinates are shown herein

The required BCs are:

$$u(x,0)=ax, v(x,0)=0, -\gamma k_f\frac{\partial T}{\partial y}(x,0)=h_f\left(T_f-T(x,0)\right) \\ u(x,\infty)=0, T_f(x,\infty)=T_\infty. \tag{4}$$

where $[u, v, 0]$ represents the velocity, g represents the gravitational acceleration, ρ is the density, μ represents the kinematic viscosity, σ stands for the electrical conductivity, c_p represents the specific heat constant, k represents the thermal ty, nf represents the nanofluid, β_{nf} is the thermal expansion coefficient and γ is the thermal slip effect.

The correlations of the nanoparticles are as follows:

$$\rho_{nf}=(1-\varphi)\rho_f+\varphi\rho_s, \beta_{nf}=(1-\varphi)\beta_f+\varphi\beta_s, \\ \mu_{nf}=\frac{\mu_f}{(1-\varphi)^{2.5}}, \\ \left(\rho c_p\right)_{nf}=(1-\varphi)\left(\rho c_p\right)_f+\varphi\left(\rho c_p\right)_s, \\ \sigma_{nf}=\sigma_f\left[1+\frac{3(r-1)\varphi}{(r+2)-(r-1)\varphi}\right], \\ r=\frac{\sigma_s}{\sigma_f}, \frac{k_{nf}}{k_f}=\frac{(k_s+2k_f)-2\varphi(k_f-k_s)}{(k_s+2k_f)+\varphi(k_f-k_s)}. \tag{5}$$

The following new variables convert Eqs. (1)–(5) into dimensionless forms:

$$u=axf'(\eta), v=-\sqrt{av_f}, \psi=\left(av_f\right)^{\frac{1}{2}}xf(\eta), \\ \eta=\left(\frac{a}{v_f}\right)^{\frac{1}{2}}y, \theta(\eta)=\frac{T-T_\infty}{T_w-T_\infty}, \tag{6}$$

And, hence, one can get:

$$f'''+\phi_1[ff''-f'^2]-[M\phi_2(1-\phi)^{2.5}+K]f'$$
$$+Gr\phi_1\left(1-\varphi+\varphi\frac{\beta_s}{\beta_f}\right)\theta=0, \quad (7)$$

$$\theta''+\frac{k_f}{k_{nf}}Pr\,\phi_3\left[f\theta'-2f'\theta+\beta^*\theta+\frac{Ec}{\phi_4}f''^2\right]+\phi_2\frac{k_fMEcPr}{k_{nf}{}'^2}. \quad (8)$$

The dimensioless BCs are:

$$\left.\begin{aligned} &f(0)=0, f'(0)=1, \theta'(0)=\frac{B_i}{\gamma}[1-\theta(0)],\\ &\theta(\infty)=0, f'(\infty)=0. \end{aligned}\right\} \quad (9)$$

The derivatives involved in Eq. (9) are with respect to the variable η. M is the magnetic parameter, Hartmann number is Ha, Grashof number is Gr, β^* is the heat generation parameter, K is porous medium parameter, Prandtl number is denoted by Pr, Ec is the Eckert number and Bi is the Biot number. These are stated as follows:

$$Gr=\frac{\beta_f g(T_f-T_\infty)}{U_0 a}, Pr=\frac{\nu_f}{\alpha_f}, M=\frac{\sigma_f {B_0}^2}{\rho_f a},$$
$$K=\frac{\nu_f}{ak_1}, \beta^*=\frac{Q}{a(\rho c_p)_{naf}}, Ec=\frac{{U_0}^2}{Cp_f T_0}, Bi=\frac{h_f}{k_f} \quad (10)$$

ϕ_1, ϕ_2, ϕ_3 and ϕ_4 are given by

$$\phi_1=(1-\phi)^{2.5}\left(1-\phi+\phi\frac{\rho_s}{\rho_f}\right), \phi_2=\left(1+\frac{3(r-1)\phi}{(r+2)-(r-1)\phi}\right),$$
$$\phi_3=\left(1-\phi+\phi\frac{(\rho c_p)_s}{(\rho c_p)_f}\right), \phi_4=(1-\phi)^{2.5}\left(1-\phi+\phi\frac{(\rho c_p)_s}{(\rho c_p)_f}\right).$$

The divergent velocity is

$$C_f=\frac{\tau_{xy|y=0}}{\rho_f U_0^2}=\frac{1}{Re_x^{\frac{1}{2}}(1-\varphi)^{2.5}}f''(0).$$

The Nusselt number is

$$Nu=\frac{xq_w}{k_f(T_f-T_\infty)}=\frac{Re_x^{\frac{1}{2}}k_{rf}}{k_f}\theta'(0).$$

The Reynolds number is $\mathrm{Re_x}=\frac{\mathrm{ax}^2}{\nu_f}$.

3. NUMERICAL APPROACH

3.1. Numerical procedure

The modelling for the exchange of heat and mass through dimensionless rules are done using the FEM. This is a groundbreaking strategy that has been used in several recent studies. The following is the process for putting FEM into practice.

a. The domain [0, ∞] is discretised into line segments such that each element has two nodes.
b. The linear weight and shape functions are given by

$$S_j=(-1)^{j-1}\left(\frac{\xi_{j+1}-\xi}{\xi_{j+1}-\xi_j}\right), i=1,2\ldots$$

c. The residual error is integrated over $[\eta_e, \eta_{e+1}]$.
d. The dependent unknowns are approximated over the element $[\eta_e, \eta_{e+1}]$ by the finite element approximations:

$$f=\sum_{j=1}^2 S_j f_j, \theta=\sum_{j=1}^2 S_j\theta_j, \phi=\sum_{j=1}^2 S_j\phi_j, h=\sum_{j=1}^2 S_j h_j,$$

where f_j, h_j, θ_j and ϕ_j are to be computed. S_j is the shape function. Hence, the stiffness elements are as follows:

$$K_{ij}^{11}=\int_{\eta_e}^{\eta_{e+1}} S_iS_j'd\eta, K_{ij}^{12}=\int_{\eta_e}^{\eta_{e+1}} -S_iS_jd\eta,$$
$$K_{ij}^{22}=\int_{\eta_e}^{\eta_{e+1}}\left(-\left(\frac{\upsilon_{hnf}}{\upsilon_f}\right)\left(1+\frac{1}{\beta}\right)S_i'S_j'-\bar{h}S_iS_j-\bar{f}(\bar{h})'S_iS_j'-M\left(\frac{\sigma_{hnf}}{\sigma_f}\right)\left(\frac{\rho_f}{\rho_{hnf}}\right)S_iS_j-KS_iS_j\right)d\eta,$$
$$K_{ij}^{23}=\int_{\eta_e}^{\eta_{e+1}}(Gr)_tS_iS_jd\eta, K_{ij}^{24}=\int_{\eta_e}^{\eta_{e+1}}(Gr)_cS_iS_jd\eta,$$
$$K_{ij}^{33}=\int_{\eta_e}^{\eta_{e+1}}\left(-\left(\frac{K_{hnf}}{K_f}\right)\left(\frac{\rho_f}{\rho_{hnf}}\right)\left(\frac{(C_p)_f}{(C_p)_{hnf}}\right)S_i'S_j'+Pr\bar{f}S_iS_j'+Pr\beta^*S_iS_j\right)d\eta,$$
$$K_{ij}^{32}=\int_{\eta_e}^{\eta_{e+1}}\left(\left(\frac{\upsilon_{hnf}}{\nu_f}\right)\left(\frac{(C_p)_f}{(C_p)_{hnf}}\right)\left(1+\frac{1}{\beta}\right)PrEc(\bar{h})'S_iS_j'+MEc\left(\frac{\sigma_{hnf}}{\sigma_f}\right)\left(\frac{(C_p)_f}{(C_p)_{hnf}}\right)+\left(\frac{\rho_f}{\rho_{hnf}}\right)PrS_iS_j\right)d\eta,$$
$$K_{ij}^{34}=\int_{\eta_e}^{\eta_{e+1}} -(PrD_f)S_i'S_j'd\eta,$$
$$K_{ij}^{44}=\int_{\eta_e}^{\eta_{e+1}} -S_i'S_j'+Sc\bar{f}S_iS_j'd\eta,$$
$$K_{ij}^{43}=\int_{\eta_e}^{\eta_{e+1}} -SrScS_i'S_j'd\eta,$$

where $\bar{f}$ and $\bar{h}$ are the computed nodal values.

e. The non-linear equations are as follows:

$$[K\{\pi\}]\{\pi\}=\{F\}.$$

These are solved using Picard linearisation as follows:

$$[K\{\pi\}^{r-1}]\{\pi\}^r=\{F\},$$

where $\{\pi\}^{r-1}$ is the nodal value computed at $(r-1)$ of the iteration and $\{\pi\}^r$ is the nodal value computed at the rth iteration.

The following equation is used to calculate the error:

$$error=\left|\frac{\pi^r-\pi^{r-1}}{\pi^{r-1}}\right|, max\left|\frac{\pi^r-\pi^{r-1}}{\pi^{r-1}}\right|<\varepsilon,$$

while taking $\varepsilon=10^{-5}$.

4. OUTCOMES AND DISCUSSION

The normalised governing boundary value problems with correlations for the thermo-physical properties are transformed into initial value problems. The transformed initial value problems with initial conditions are solved by FEM.

The parametric simulations are then conducted to examine the dynamics of the flow variables. Simulations are run to select the nanoparticles among $\mathrm{CuO}, \mathrm{Al_2O_3}$ and $\mathrm{TiO_2}$ so that the system works in an efficient manner. Fig. 2 shows the velocity profiles of copper nanofluids, aluminium nanofluids and titanium nanofluids when Gr =0.2 and 0.5. This figure explains that the velocity of titanium nanofluid achieves the highest value, compared to CuO nanofluid and all nanofluids, for both cases when Gr =0.2 and 0.5. This figure also explains that the velocity of copper nanofluids, aluminium nanofluids and titanium nanofluids increases on

increasing the magnitude of Gr. The Grashof number is significant because it shows the ratio of the buoyant force caused by spatial variations in fluid density (induced by temperature differences) to the restraining force caused by the fluid's viscosity.

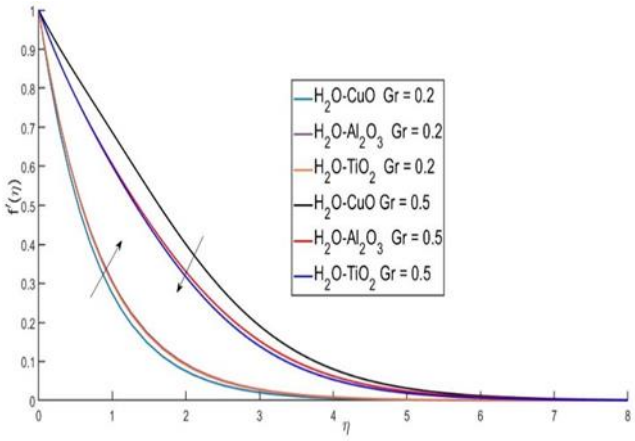

Fig. 2. Velocity profile against favourable buoyant force

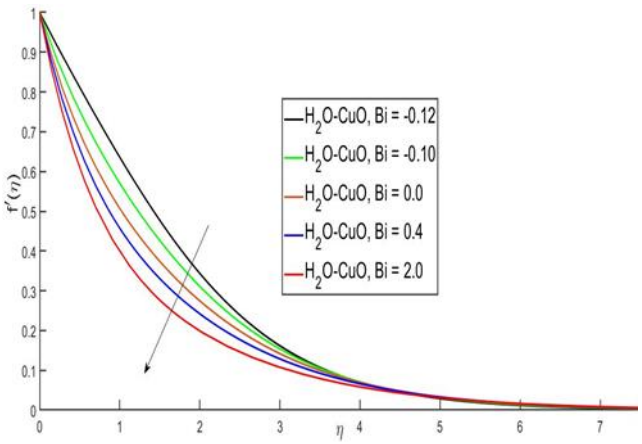

Fig. 3. Velocity profile against Biot number

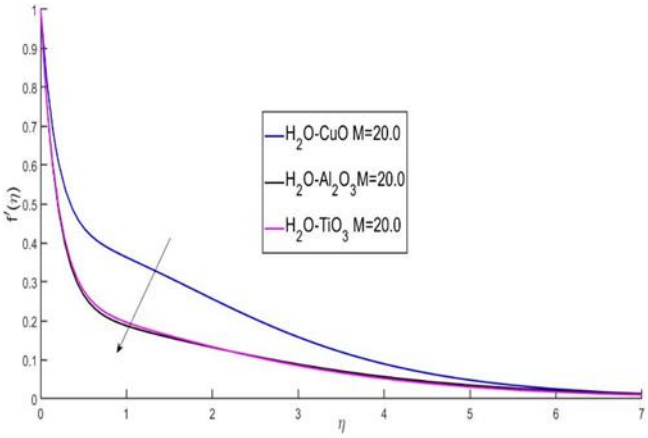

Fig. 4. Velocity profile against magnetic field

Fig. 3 shows the effects of the Biot number Bi on velocity. On increasing the value of the Biot number, the velocity decreases. Because the Biot number is significant, it is used to calculate the heat transfer rate. In Fig. 4, it is noted that on increasing the magnetic field parameter M, the boundary layer's viscosity decreases due to the application of the magnetic field on the particles of an electrical conducting fluid, causing a Lorentz force in the boundary layer. The Hall effect uses magnetic forces to reveal information about charge carriers in a substance.

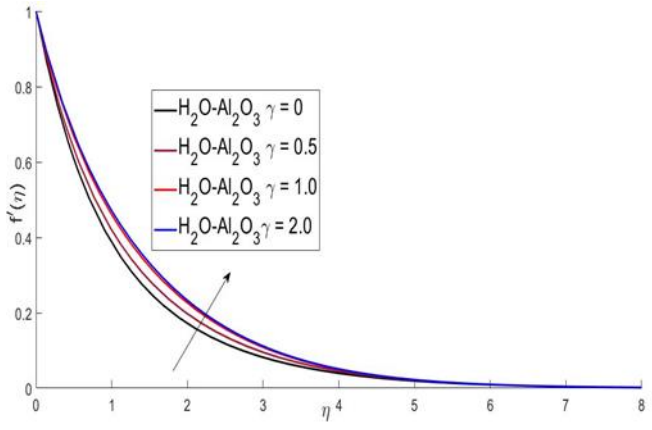

Fig. 5. Velocity profile against thermal effect

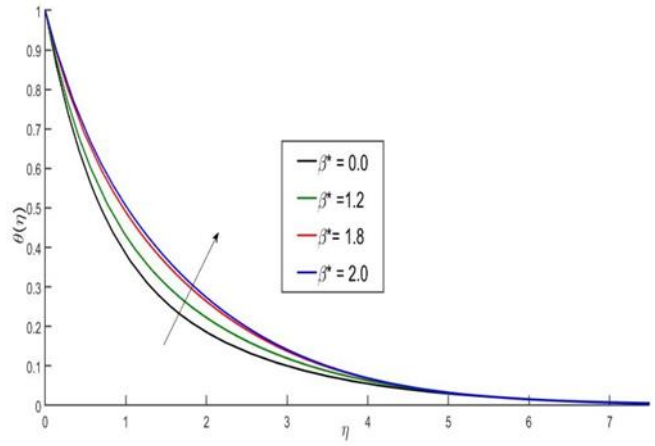

Fig. 6. Temperature profile against heat generation

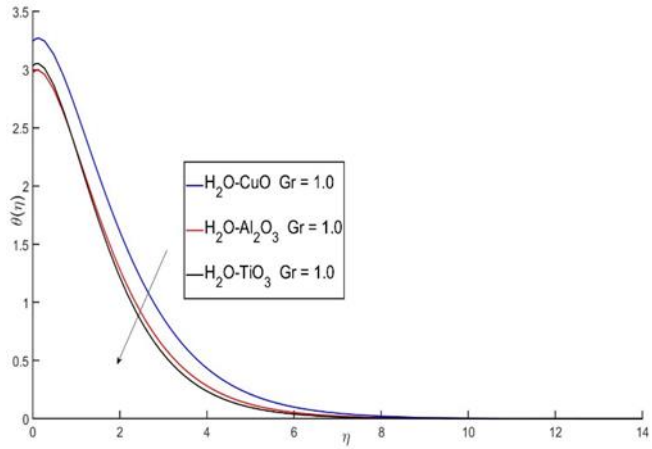

Fig. 7. Temperature profile aginst favourable buoyant force

Fig. 5 presents the velocity profile in relation to thermal effects; it shows that on increasing the values of thermal effects, the velocity profile increases. Fig. 6 illustrates the influence of the heat generation parameter β^* on temperature. It is observed that

on increasing the value of Ec, the boundary layer thickness also increases. In Fig. 7, we see the effects of Gr on temperature; we observed that when we increase the value of Gr , the temperature increases.

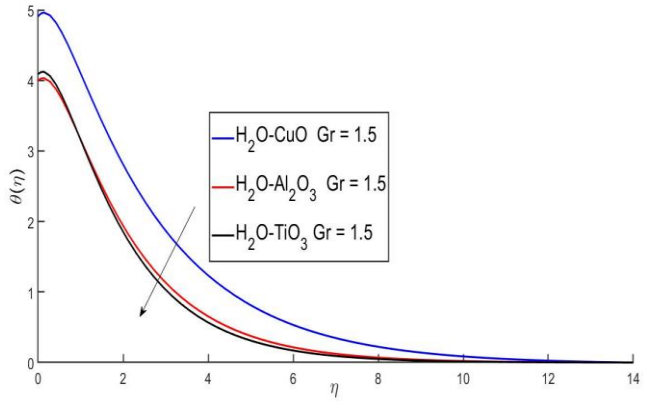

Fig. 8. Temperature profile against favourable buoyant force

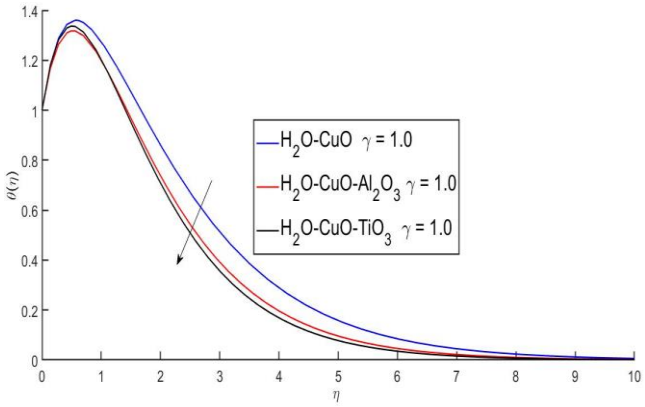

Fig. 9. Temperature profile against thermal effects

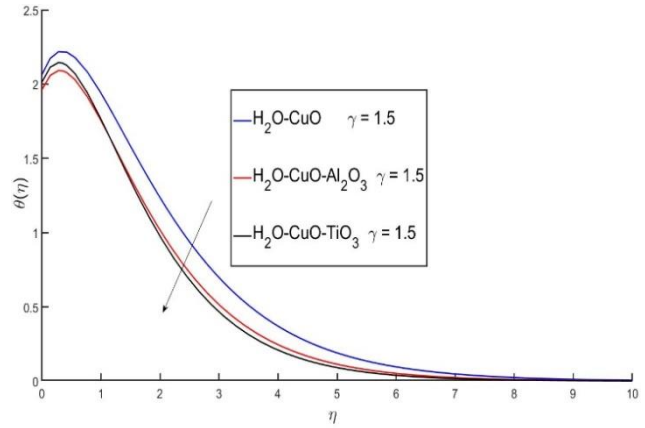

Fig. 10. Temperature profile against thermal effects

Fig. 8 shows the compression of Gr on temperature in the fluids comprising copper–water, aluminium–water and titanium–water. We notice that the viscosity of the boundary layer decreases on increasing the content of nanofluids. Figs. 9–11 show the impacts of the thermal slip parameter γ on temperature considering copper–water, aluminium–water and titanium–water nanofluids. It is observed that temperature diminishes on increasing the value of γ. The copper nanofluid is more heat effective as compared to other nanofluids, namely aluminium and titanium nanofluids. The thermophysical properties of water and nanoparticles are presented in Tab. 1. The local skin friction coefficient and Nusselt number for copper oxide–water nanofluid with different nanoparticle factors are presented in Tab. 2.

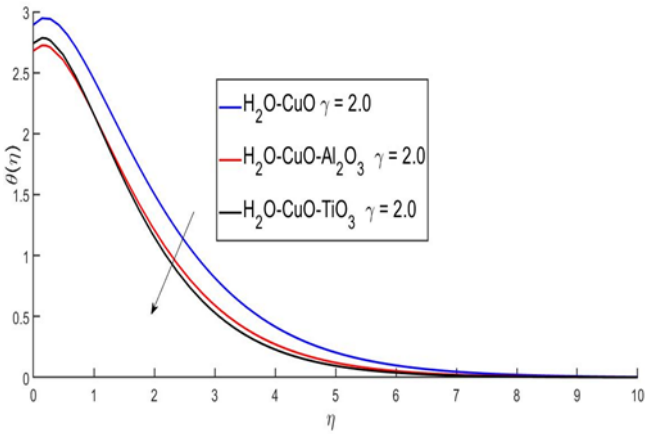

Fig. 11. Temperature profile against thermal effects

Tab. 1. Thermophysical properties of water and nanoparticles [33]

Materials	$\rho\ (kg/m^3)$	$c_p(J/kgK)$	$k\ (W/mK)$	$\beta\times10^{-5}\ (K^{-1})$	$\sigma\ (S/m)$
Water (H_2O)	997.5	4,178.0	0.6280	21.40	5.5×10^{-6}
Copper oxide (CuO) nanoparticles	6,310.0	550.5	32.90	0.85	5.96×10^{7}
Aluminium oxide (Al_2O_3) nanoparticles	3,900.0	779.0	40.00	0.84	3.50×10^{7}
Titanium oxide (TiO_2) nanoparticles	4,250.0	686.2	8.9538	0.90	2.38×10^{6}

Tab. 2. Local skin friction coefficient and Nusselt number for copper oxide–water nanofluid with different nanoparticle factors at ϕ =0.2 [33]

k_{nf}	$Re_x^{-1/2}\,Nu$	$Re_x^{-1/2}\,Nu$
0.628	0.084138154	0.993989767
0.72141	0.085608603	1.18560452
0.82458	0.086968704	1.381935016
0.9391	0.091634371	1.58355532
1.06696	0.095644211	1.79198143

5. CONCLUSION

Convection heat transfer in Newtonian fluids containing nano-solid metallic structures has been studied to investigate the enhancement in thermal conductivity, so that dispersion of nanoparticles of copper oxide, aluminium oxide, and titanium oxide may be recommended for an efficient thermal system such as automobile engines. The boundary layer's governing problems are numerically solved, and the significant studies are included.

When the Grashof number is increased, the favourable buoyancy force aids the flow, and the thickness of the MHD boundary

layer shows an increasing trend. This research is applicable for all kinds of nanoparticles.

On the flow of fluids, the fluctuation in Biot number results in a declining trend. As a result, as the Biot number increases, the flow slows down.

REFERENCES

1. Khan WA, Aziz A. Double-diffusive natural convective boundary layer flow in a porous medium saturated with a nanofluid over a vertical plate: Prescribed surface heat, solute and nanoparticle fluxes. International Journal of Thermal Sciences. 2011;50(11):2154-60.
2. Hayat T, Khan MI, Waqas M, Alsaedi A, Farooq M. Numerical simulation for melting heat transfer and radiation effects in stagnation point flow of carbon–water nanofluid. Computer methods in applied mechanics and engineering. 2017;315:1011-24.
3. Maghsoudi P, Siavashi M. Application of nanofluid and optimization of pore size arrangement of heterogeneous porous media to enhance mixed convection inside a two-sided lid-driven cavity. Journal of Thermal Analysis and Calorimetry. 2019;135(2):947-61.
4. Sheikholeslami M, Zeeshan A. Numerical simulation of Fe3O4-water nanofluid flow in a non-Darcy porous media. International Journal of Numerical Methods for Heat & Fluid Flow. 2018;28(3):641-60.
5. Hanif H, Khan I, Shafie S. MHD natural convection in cadmium telluride nanofluid over a vertical cone embedded in a porous medium. Physica Scripta. 2019;94(12):125208.
6. Vo DD, Hedayat M, Ambreen T, Shehzad SA, Sheikholeslami M, Shafee A, Nguyen TK. Effectiveness of various shapes of Al 2 O 3 nanoparticles on the MHD convective heat transportation in porous medium. Journal of Thermal Analysis and Calorimetry. 2019;1-9.
7. Ismail AI. Finite element simulation of magnetohydrodynamic convective nanofluid slip flow in porous media with nonlinear radiation. *Alexandria Eng. J.* 2016; *55*:1305–1319.
8. Saleem S, Shafee A, Nawaz M, Dara RN, Tlili I, Bonyah E. Heat transfer in a permeable cavity filled with a ferrofluid under electric force and radiation effects. AIP Advances. 2019;9(9):095107.
9. Alharbi SO, Nawaz M, Nazir U. Thermal analysis for hybrid nanofluid past a cylinder exposed to magnetic field. AIP Advances. 2019;9(11):115022.
10. Ghadikolaei SS, Hosseinzadeh K, Ganji DD, Hatami M. Fe3O4–(CH2OH) 2 nanofluid analysis in a porous medium under MHD radiative boundary layer and dusty fluid. Journal of Molecular Liquids. 2018;258:172-85.
11. Nawaz M, Rana S, Qureshi IH. Computational fluid dynamic simulations for dispersion of nanoparticles in a magnetohydrodynamic liquid: a Galerkin finite element method. RSC advances. 2018;8(67):38324-35.
12. Nawaz M, Rana S, Qureshi IH, Hayat T. Three-dimensional heat transfer in the mixture of nanoparticles and micropolar MHD plasma with Hall and ion slip effects. AIP Advances. 2018;8(10):105109.
13. Hatami M, Hosseinzadeh K, Domairry G, Behnamfar MT. Numerical study of MHD two-phase Couette flow analysis for fluid-particle suspension between moving parallel plates. Journal of the Taiwan Institute of Chemical Engineers. 2014;45(5):2238-45.
14. Ali B, Nie Y, Khan SA, Sadiq MT, Tariq M. Finite element simulation of multiple slip effects on MHD unsteady Maxwell nanofluid flow over a permeable stretching sheet with radiation and thermo-diffusion in the presence of chemical reaction. Processes. 2019;7:1–18.
15. Balla CS, Naikoti K. Finite element analysis of magnetohydrodynamic transient free convection flow of nanofluid over a vertical cone with thermal radiation. Proc. Inst. Mech. Eng. Part N J. Nanoeng. Nanosyst. 2016;*230*:161–173.
16. Li Z, Sheikholeslami M, Mittal AS, Shafee A, Haq RU. Nanofluid heat transfer in a porous duct in the presence of Lorentz forces using the lattice Boltzmann method. The European Physical Journal Plus. 2019;134(1):30.
17. Sheikholeslami M, Saleem S, Shafee A, Li Z, Hayat T, Alsaedi A, Khan MI. Mesoscopic investigation for alumina nanofluid heat transfer in permeable medium influenced by Lorentz forces. Computer Methods in Applied Mechanics and Engineering. 2019;349:839-58.
18. Saleem S, Firdous H, Nadeem S, Khan AU. Convective heat and mass transfer in magneto Walter's B nanofluid flow induced by a rotating cone. Arabian Journal for Science and Engineering. 2019;44(2):1515-23.
19. Sadiq MA, Khan AU, Saleem S, Nadeem S. Numerical simulation of oscillatory oblique stagnation point flow of a magneto micropolar nanofluid. RSC advances. 2019;9(9):4751-64.
20. Ramzan M, Sheikholeslami M, Saeed M, Chung JD. On the convective heat and zero nanoparticle mass flux conditions in the flow of 3D MHD Couple Stress nanofluid over an exponentially stretched surface. Scientific reports. 2019;9(1):562.
21. Dogonchi AS, Armaghani T, Chamkha AJ, Ganji DD. Natural Convection Analysis in a Cavity with an Inclined Elliptical Heater Subject to Shape Factor of Nanoparticles and Magnetic Field. Arabian Journal for Science and Engineering. 2019:1-3.
22. Saleem S, Nadeem S, Rashidi MM, Raju CS. An optimal analysis of radiated nanomaterial flow with viscous dissipation and heat source. Microsystem Technologies. 2019;25(2):683-9.
23. Dogonchi AS, Waqas M, Seyyedi SM, Hashemi-Tilehnoee M, Ganji DD. Numerical simulation for thermal radiation and porous medium characteristics in flow of CuO-H 2 O nanofluid. Journal of the Brazilian Society of Mechanical Sciences and Engineering. 2019;41(6):249.
24. Gholinia M, Hosseinzadeh K, Mehrzadi H, Ganji DD, Ranjbar AA. Investigation of MHD Eyring–Powell fluid flow over a rotating disk under effect of homogeneous–heterogeneous reactions. Case Studies in Thermal Engineering. 2019;13:100356.
25. Hosseinzadeh K, Gholinia M, Jafari B, Ghanbarpour A, Olfian H, Ganji DD. Nonlinear thermal radiation and chemical reaction effects on Maxwell fluid flow with convectively heated plate in a porous medium. Heat Transfer—Asian Research. 2019;48(2):744-59.
26. Afridi MI, Qasim M, Saleem S. Second law analysis of three dimensional dissipative flow of hybrid nanofluid. Journal of Nanofluids. 2018;7(6):1272-80.
27. Chamkha AJ, Dogonchi AS, Ganji DD. Magneto-hydrodynamic flow and heat transfer of a hybrid nanofluid in a rotating system among two surfaces in the presence of thermal radiation and Joule heating. AIP Advances. 2019;9(2):025103.
28. Zangooee MR, Hosseinzadeh K, Ganji DD. Hydrothermal analysis of MHD nanofluid (TiO2-GO) flow between two radiative stretchable rotating disks using AGM. Case Studies in Thermal Engineering. 2019;14:100460.
29. Sheikholeslami M, Jafaryar M, Barzegar GM, Alavi AH.Influence of novel turbulator on efficiency of solar collector system. Environmental Technology and Innovation. 2022;26:102383.
30. Sheikholeslami M, Ebrahimpour Z. Thermal improvement of linear Fresnel solar system utilizing Al2O3-water nanofluid and multi-way twisted tape, International Journal of Thermal Sciences. 2022;176:107505.
31. Sheikholeslami M, Farshad SA, Gerdroodbary MB, Alavi AH. Impact of new multiple twisted tapes on treatment of solar heat exchanger. The European Physical Journal Plus. 2022;137:86.
32. Zeeshan A, Shehzad N, Atif M, Ellahi R, Sait SM. Electromagnetic Flow of SWCNT/MWCNT Suspensions in Two Immiscible Water-and Engine-Oil-Based Newtonian Fluids through Porous Media. Symmetry. 2022;14(2):406.
33. Hafeez MB, Amin R, Nisar KS, Jamshed W, Abdel-Aty AH, Khashan MM, Heat transfer enhancement through nanofluids with applications in automobile radiator, Case Studies in Thermal Engineering. 2021;27:101192.

34. Bhatti MM, Arain MB, Zeeshan A, Ellahi R, Doranehgard MH. Swimming of Gyrotactic Microorganism in MHD Williamson nanofluid flow between rotating circular plates embedded in porous medium: Application of thermal energy storage. Journal of Energy Storage. 2022;45:103511.
35. Khan AA, Ilyas S, Abbas T, Ellahi R. Significance of induced magnetic field and variable thermal conductivity on stagnation point flow of second grade fluid. Journal of Central South University. 2021;28(11):3381-90.

Muhammad Bilal Hafeez: https://orcid.org/0000-0002-9384-8582
Marek Krawczuk: https://orcid.org/0000-0002-9640-4696
Hasan Shahzad: https://orcid.org/0000-0001-9154-5791

NOMENCLATURES

C_{p}	Specific heat constant
Nu_{x}	Local Nusselt number
C_{f}	Skin friction coefficient
nf	Nanofluid
h_{f}	Heat transfer coefficient
k	Thermal conductivity of base fluid
q	Heat flux
q_{w}	Surface heat flux
T	Temperature of base fluid
u	Horizontal velocity field components
v	Vertical velocity field components
Bi	Biot number
Ec	Eckert number
Pr	Prandtl number
g	Gravitational acceleration
B_0	Magnetic field parameter

GREEK SYMBOLS

β_{S}	Thermal expansion coefficient
σ	Boltzmann constant
φ	Volume fraction of nanoparticles
γ	Slip parameter
λ	Thermal relaxation time
μ	Density of fluid
μ_{nf}	Kinematic viscosity of nanofluid
v	Kinematic viscosity of base fluid
ρ	Density of base fluid
τ_{w}	Density of nanoparticle
τ_{w}	Surface skin friction